Rizov *International Journal of Mechanical and Materials Engineering* (2017) 12:4
DOI 10.1186/s40712-017-0073-7

International Journal of Mechanical and Materials Engineering

ORIGINAL ARTICLE Open Access

Delamination fracture analysis of an elastic-plastic functionally graded multilayered beam

V. Rizov

Abstract

Background: A theoretical study was performed of mode II delamination in a multilayered functionally graded beam configuration with considering the material non-linearity.

Methods: The fracture was analysed by the *J*-integral approach. Two laws (quadratic and exponential) for variation of the modulus of elasticity along the beam height were applied. The *J*-integral closed form non-linear analytical solutions derived were verified by performing analyses of the strain energy release rate with taking into account the material non-linearity. Parametric investigations of mode II non-linear fracture were conducted.

Results: It was found that material non-linearity leads to increase of the *J*-integral value. Therefore, the non-linear behaviour of material has to be taken into account in fracture mechanics-based safety design of functionally graded structural members.

Conclusions: The present paper contributes to the understanding of non-linear fracture in functionally graded materials. The results obtained can be used for optimization of functionally graded beam structures with respect to the fracture performance.

Keywords: Functionally graded beam, Material non-linearity, Delamination fracture, Analytical approach

Background

Functionally graded materials are new composites developed in the last 30 years (Ashrafi and Shariyat 2014; Bohidar et al. 2014; Butcher et al. 1999; Gasik 2010; Hirai and Chen 1999; Ivanov and Stoyanov 2011; Lu et al. 2009; Maganti and Nalluri 2015; Mohammadiha and Ghariblu 2016; Mortensen and Suresh 1995; Nemat-Allal et al. 2011; Neubrand and Rödel 1997; Suresh and Mortensen 1998). They are made by mixing of two or more material constituents in different ratios in different parts of a structural member in order to get optimum performance to external loads. The most important advantage of the functionally graded materials over the laminated composites (Szekrenyes 2010; Szekrenyes and Vicente 2012) is that the composition of the former changes gradually along one or more spatial coordinates. In this way, boundary surfaces and sharp interfaces between different constituent materials are eliminated. Thus, failures from interfacial stress concentrations are avoided. The engineering practice shows that very often, fracture is the critical failure mode in structural members composed by functionally graded materials. Therefore, the study of fracture behaviour is very important for further advancement of functionally graded material technologies (Carpinteri and Pugno 2006; Erdogan 1995; Paulino 2002; Pei and Asaro 1997; Shi-Dong Pan et al. 2009; Tilbrook et al. 2005; Upadhyay and Simha 2007).

Fracture behaviour has been studied of a strip of a functionally graded material subjected to edge loading consisting of axial forces and bending moments by Pei and Asaro 1997. The methods of linear-elastic fracture mechanics have been applied. Analytical solutions have been derived for stress intensity factors. The investigation performed has revealed that the material gradients have significant influence on the fracture behaviour.

Correspondence: V_RIZOV_FHE@UACG.BG
Department of Technical Mechanics, University of Architecture, Civil Engineering and Geodesy, 1 Chr. Smirnensky blvd., 1046 Sofia, Bulgaria

Recent studies of the fracture in functionally graded composites have been reviewed by Tilbrook et al. 2005. Various solutions for stress intensity factors have been presented. Cracks propagating parallel or perpendicular to material gradient direction have been analysed assuming linear-elastic behaviour. The strain energy release rate has been investigated for periodic cracks in functionally graded materials. Effects of material property variation on fracture behaviour have been discussed.

Evaluation has been performed of the strength of structures composed by linear-elastic functionally graded materials incorporating re-entrant corners by Carpinteri and Pugno 2006. An analytical method has been developed for predicting the strength of structural members corresponding to the unstable brittle crack propagation. The validity of the method has been proved by considering plates under tension and beams under bending.

The compliance approach has been applied for calculation of stress intensity factors in functionally graded beams subjected to three-point bending assuming linear-elastic material behaviour (Upadhyay and Simha 2007). An equivalent beam of variable height has been suggested for engineering design analysis of the cracked functionally graded beam. It has been demonstrated that the equivalent compliance concept is particularly suitable for cracked structural members loaded by concentrated forces.

Although many researchers have investigated the fracture in functionally graded structural members, there are still crack problems that have not been studied sufficiently (for instance, fracture behaviour of functionally graded beams exhibiting material non-linearity). Therefore, the purpose of present paper was to perform a theoretical study of mode II delamination fracture in a functionally graded multilayered beam with considering the material non-linearity. It should be mentioned that the present paper was motivated also by the fact that functionally graded materials can be built up layer by layer (Bohidar et al. 2014) which is a premise for appearance of delamination cracks between layers. In real functionally graded structures, delamination cracks can be loaded in different modes due to the big variety of structural geometries and external loadings and influences. Mode II crack loading conditions are induced by in-plane shear. Delamination cracks in functionally graded layered materials are studied usually for mode I case, because the mode I fracture toughness is the lowest. However, with complex loading conditions seen in service, mode II delamination may occur too. Beside, in tougher layered systems, the difference between mode I and mode II fracture toughness decreases which also indicates the need of analysing mode II delamination cracks. In the present paper, the fracture was investigated by applying the *J*-integral approach. The closed form analytical solutions derived were verified by performing strain energy release rate analyses with taking into account the material non-linearity. Effects were evaluated of the material properties and crack location on the fracture behaviour. The present paper contributes towards the understanding of non-linear fracture in functionally graded materials.

Methods

First, fracture behaviour of the three-layered functionally graded beam shown schematically in Fig. 1 was analysed in the present paper. There are two symmetric delamination cracks of length, a, between the layers. A tensile force, F, is applied centrically at the free end of internal crack arm. In this way, mode II crack loading is induced (it should be noted that similar beam configuration has been used to study mode II delamination fracture in laminated composites (Mladensky and Rizov 2013)). It is obvious that the two external crack arms are free of stresses. The beam cross section is a rectangle of width, b, and height, h. The internal crack arm thickness is $2h_2$. The beam is clamped in the right-hand end. It was assumed that the material is functionally graded along the beam height symmetrically with respect to the centroid. In the analysis, only the upper half of the beam, $-h/2 \le z_1 \le 0$, was considered due to the symmetry.

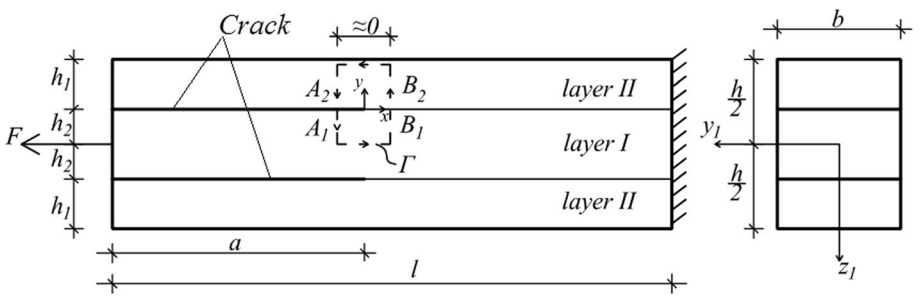

Fig. 1 The geometry of a beam with two symmetric delamination cracks

The fracture behaviour was analysed by applying the *J*-integral approach. For functionally graded materials, the *J*-integral was formulated as (Anlas et al. 2000)

$$J = \int_{\Gamma} \left[u_0 \cos\alpha - \left(p_x \frac{\partial u}{\partial x} + p_y \frac{\partial v}{\partial x} \right) \right] ds - \int_{A} \frac{\partial u_0}{\partial x} q dA, \tag{1}$$

where Γ is a contour of integration going from the lower crack face to the upper crack face in the counter clockwise direction, u_0 is the strain energy density, α is the angle between the outwards normal vector to the contour of integration and the crack direction, p_x and p_y are the components of the stress vector, u and v are the components of the displacement vector with respect to the crack tip coordinate system xy (x is directed along the crack), ds is a differential element along the contour, A is the area enclosed by that contour, and q is a weight function with a value of unity at the crack tip, zero along the contour and arbitrary elsewhere. It should be specified that the partial derivative, $\partial u_0/\partial x$, exists only if the material property is an explicit function of x (Anlas et al. 2000).

It should also be noted that the present fracture study is based on the small strain assumption.

The integration was performed along the contour, Γ, that consists of the beam cross sections ahead and behind the crack tip (Fig. 1). It was mentioned above that the upper crack arm is stress free. Therefore, the *J*-integral value in the upper crack arm is zero. The *J*-integral solution was written as

$$J = 2\left(J_{A_1} + J_{B_1} + J_{B_2} \right), \tag{2}$$

where J_{A1}, J_{B1} and J_{B2} are the *J*-integral values in segments A_1, B_1 and B_2, respectively. Segment A_1 coincides with the upper half of the cross section of internal crack arm behind the crack tip. Segment B_1 coincides with the upper half of cross section of internal layer *I* ahead of the crack tip, and segment B_2 coincides with the cross section of the external layer *II* ahead of the crack tip. It should be noted that the expression in brackets in (2) is doubled, because there are two symmetric cracks in the beam considered (Fig. 1).

It was assumed that the modulus of elasticity, E_c, of the internal layer *I* varies continuously in the thickness direction according to the following quadratic law:

$$E_c(z_1) = E_{c0} + \frac{E_{c1} - E_{c0}}{h_2^2} z_1^2 \text{ at } -h_2 \le z_1 \le h_2, \tag{3}$$

where E_{c0} and E_{c1} are the values of E_c in the beam cross-sectional centre and in the internal layer edge, respectively.

The modulus of elasticity, E_f, of the external layer *II* varies through the thickness as

$$E_f(z_1) = E_{f0} + \frac{E_{f1} - E_{f0}}{h_1^2} (h_2 + z_1)^2 \text{ at } -h_1 - h_2 \le z_1 \le -h_2, \tag{4}$$

where E_{f0} and E_{f1} are the values of the modulus of elasticity in the lower and in the upper edge of layer *II*, respectively. Here, h_1 is the thickness of layer *II* (Fig. 1).

First, a linear-elastic fracture analysis was performed. The *J*-integral components in segment A_1 were written as

$$p_x = -\sigma, p_y = 0, \quad ds = dz_1, \cos\alpha = -1, \tag{5}$$

where the z_1-coordinate varies in the interval $[-h_2, 0]$. According to Hooke's law, the stress, σ, was expressed as

$$\sigma = E_c(z_1)\varepsilon_c. \tag{6}$$

The following equation for equilibrium was used to derive the longitudinal strain, ε_c, in the internal crack arm behind the crack tip:

$$\frac{F}{2} = \int_{-h_2}^{0} \sigma b dz_1. \tag{7}$$

From (4), (6) and (7), we obtained

$$\varepsilon_c = \frac{3F}{2bh_2(2E_{c0} + E_{c1})}. \tag{8}$$

The strain energy density was expressed as

$$u_0 = \frac{1}{2} E_c(z_1)\varepsilon_c^2. \tag{9}$$

The following equation from mechanics of materials was applied to determine the partial derivative, $\partial u/\partial x$, in (1):

$$\frac{\partial u}{\partial x} = \varepsilon_c. \tag{10}$$

The partial derivative, $\partial u_0/\partial x$, in the second integral in (1) was written as

$$\frac{\partial u_0}{\partial x} = 0, \tag{11}$$

since the strain energy density does not depend explicitly on x (the modulus of elasticity is not a function of x, because the material is functionally graded along to the beam height only (refer to (3)).

By combining (1), (3), (5), (6), (9), (10) and (11), we derived

$$J_{A_1} = \frac{1}{6}\varepsilon_c^2 h_2(2E_{c0} + E_{c1}). \tag{12}$$

The integration in segment B_1 of the integration contour (Fig. 1) was performed in the following way. The J-integral components were written as

$$p_x = \sigma, p_y = 0,\ \ ds = -dz_1,\ \cos\alpha = 1, \tag{13}$$

where z_1 varies in the interval $[0,\ -h_2]$. The stress, σ, was expressed by using Hooke's law as

$$\sigma = E_c(z_1)\varepsilon_d. \tag{14}$$

The longitudinal strain, ε_d, in the un-cracked beam portion, $x \geq 0$, was found from the following equilibrium equation:

$$\frac{F}{2} = \int_{-h_1-h_2}^{-h_2} \sigma_f b dz_1 + \int_{-h_2}^{0} \sigma_c b dz_1, \tag{15}$$

where σ_f and σ_c are the stresses in the layers II and I, respectively. These stresses were expressed by Hooke's law:

$$\sigma_f = E_f(z_1)\varepsilon_d, \tag{16}$$

$$\sigma_c = E_c(z_1)\varepsilon_d. \tag{17}$$

By combining (3), (4), (15), (16) and (17), we found

$$\varepsilon_d = \frac{3F}{2bh_1\left(2E_{f0} + E_{f1}\right) + 2bh_2(2E_{c0} + E_{c1})}. \tag{18}$$

The other J-integral components were obtained as

$$u_0 = \frac{1}{2}E_c(z_1)\varepsilon_d^2, \frac{\partial u}{\partial x} = \varepsilon_d. \tag{19}$$

From (1), (3), (4), (13), (14), (18) and (19), we obtained

$$J_{B_1} = -\frac{1}{6}\varepsilon_d^2 h_2(2E_{c0} + E_{c1}). \tag{20}$$

The J-integral components in segment B_2 of the integration contour (Fig. 1) were determined by (13), where z_1 varies in the interval $[-h_2,\ -h_1 - h_2]$ and the stress, σ, was obtained by (17). The other components were determined by (19), where $E_c(z_1)$ was replaced with $E_f(z_1)$. By combining (1), (13), (17) and (19), we derived

$$J_{B_2} = -\frac{\varepsilon_d^2}{6h_1^2}\left[3h_1^3E_{f0} + \left(E_{f1}-E_{f0}\right)h_2^3 + \left(E_{f1}-E_{f0}\right)(h_1-h_2)^3\right]. \tag{21}$$

Finally, (12), (20) and (21) were substituted in (2):

$$J = \frac{1}{3}\varepsilon_c^2 h_2(2E_{c0} + E_{c1}) - \frac{1}{3}\varepsilon_d^2 h_2(2E_{c0} + E_{c1}) - \frac{\varepsilon_d^2}{3h_1^2}\left[3h_1^3E_{f0} + \left(E_{f1}-E_{f0}\right)h_2^3 + \left(E_{f1}-E_{f0}\right)(h_1-h_2)^3\right], \tag{22}$$

where ε_c and ε_d were determined by (8) and (18), respectively.

Fracture analyses of the three-layered functionally graded beam (Fig. 1) were performed also assuming non-linear material behaviour. The mechanical behaviour of layer I was described by the following non-linear stress-strain relation (Petrov 2014):

$$\sigma = \frac{E\varepsilon}{\sqrt{1 + \left(\frac{\varepsilon}{t}\right)^2}}, \tag{23}$$

where E is obtained by (3), σ is the stress, ε is the strain, and t is a material property (usually, t is equal to unit (Petrov 2014)). The non-linear stress-strain curve is shown schematically in Fig. 2. It should be specified that the stress-strain relation (23) describes elastic-plastic behaviour with hardening that is typical for some functionally graded materials (for instance, zircona-titanium functionally graded material (Tsukamoto 2014)).

Equation (23) was applied also to describe the mechanical behaviour of layer II (the only difference is that E is determined by (4)).

It should be noted that the present non-linear fracture analysis holds for non-linear elastic material behaviour. However, the analysis is applicable also for elastic-plastic behaviour, if the external load magnitude increases only,

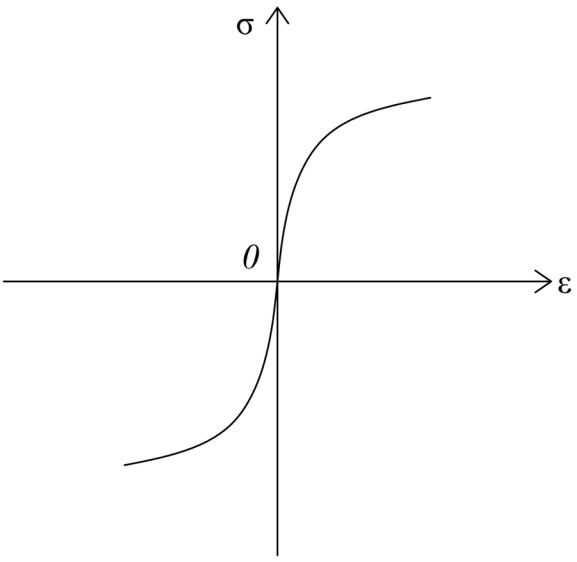

Fig. 2 Non-linear stress-strain diagram

i.e. if the functionally graded beam considered undergoes active deformation (Chakrabarty 2006).

The non-linear fracture was analysed by applying the *J*-integral approach (1). The integration was performed along the same integration contour, *Γ*, used in the linear-elastic solution (Fig. 1).

The *J*-integral components in segment A_1 of the integration contour (Fig. 1) were obtained by (5), where σ was calculated by (23). The strain, ε_c, in the internal crack arm behind the crack tip was determined by Eq. (7). By combining (3), (7) and (23), we derived

$$\varepsilon_c = \frac{t\omega}{\sqrt{t^2-\omega^2}}, \omega = \frac{3F}{2bh_2(2E_{c0}+E_{c1})}. \tag{24}$$

The strain energy density is equal to the area, *OPQ*, enclosed by the stress-strain curve (refer to Fig. 3):

$$u_0 = \int_0^{\varepsilon} \sigma d\varepsilon. \tag{25}$$

From (23) and (25), we obtained

$$u_0 = Et^2\left[\sqrt{1+\left(\frac{\varepsilon}{t}\right)^2}-1\right]. \tag{26}$$

Equation (10) was used to find the partial derivative, $\partial u/\partial x$, where ε_c was calculated by (24).

By combining (1), (3), (10), (11), (23), (24) and (26), we derived

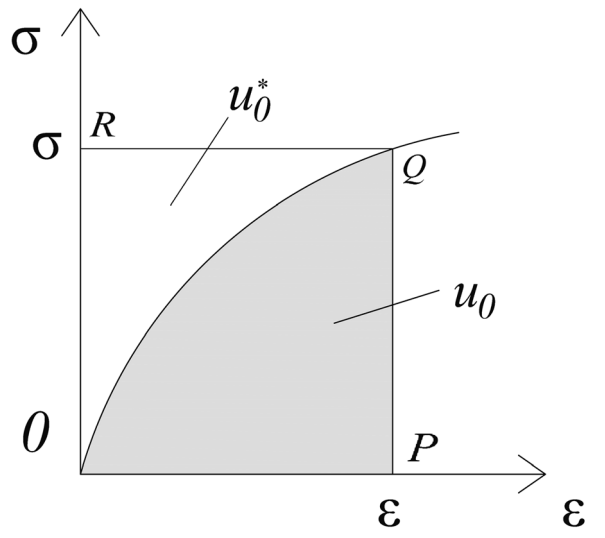

Fig. 3 Strain energy density, u_0, and complimentary strain energy density, u_0^*

$$J_{A_1} = t^2\left[1-\frac{1}{\sqrt{1+\left(\frac{\varepsilon_c}{t}\right)^2}}\right]\frac{h_2}{3}\left(2E_{c0}+E_{c1}\right). \tag{27}$$

Equation (13) was applied in order to find the *J*-integral components in segment B_1 of the integration contour (σ was obtained substitution of (3) in (23)).

The strain energy density was found by (26). For this purpose, ε was replaced with ε_d.

The strain, ε_d, in the un-cracked beam portion was found by (15). For this purpose, σ_c and σ_f were obtained by substitution of (3) and (4) in (23). In this way, from (15), we derived

$$\varepsilon_d = \frac{t\phi}{\sqrt{t^2-\phi^2}}, \phi = \frac{3F}{2bh_1\left(2E_{f0}+E_{f1}\right)+2bh_2(2E_{c0}+E_{c1})}. \tag{28}$$

By combining (1), (13), (12), (16), (23), (26) and (28), we derived

$$J_{B_1} = t^2\left[\frac{1}{\sqrt{1+\left(\frac{\varepsilon_d}{t}\right)^2}}-1\right]\frac{h_2}{3}\ \left(2E_{c0}+E_{c1}\right). \tag{29}$$

The *J*-integral components in segment B_2 of the integration contour (Fig. 1) were obtained by (13), where the stress, σ, was calculated by substitution of (4) in (23). Equation (26) was used to determine the strain energy density. For this purpose, ε was replaced with ε_d.

From (1), (4), (10), (11), (13), (23) and (26), we obtained

$$J_{B_2} = t^2\left[\frac{1}{\sqrt{1+\left(\frac{\varepsilon_d}{t}\right)^2}}-1\right]\frac{h_1}{3}\ \left(2E_{f0}+E_{f1}\right). \tag{30}$$

Equations (27), (29) and (30) were substituted in (2):

$$J = 2t^2\left[1-\frac{1}{\sqrt{1+\left(\frac{\varepsilon_c}{t}\right)^2}}\right]\frac{h_2}{3}\left(2E_{c0}+E_{c1}\right) + \frac{2}{3}t^2\left[\frac{1}{\sqrt{1+\left(\frac{\varepsilon_d}{t}\right)^2}}-1\right]\left[h_2\ \left(2E_{c0}+E_{c1}\right)+\ h_1\left(2E_{f0}+E_{f1}\right)\right], \tag{31}$$

where ε_c and ε_d were calculated by (24) and (28), respectively.

In order to verify the *J*-integral non-linear solution (31), an analysis was developed of the strain energy release rate, *G*, with taking into account the material non-linearity. The strain energy release rate, associated with an elementary increase of the crack area, dA_a, was written as

$$G = \frac{dW_{\text{ext}} - dU}{dA_a}. \tag{32}$$

The change of the external work, dW_{ext}, was expressed as

$$dW_{\text{ext}} = dU^* + dU, \tag{33}$$

where dU^* and dU are the changes of complimentary strain energy and the strain energy, respectively. By combining (32) and (33), we obtained

$$G = \frac{dU^*}{dA_a}, \tag{34}$$

where

$$dA_a = bda. \tag{35}$$

Here, da is an elementary crack length increase.

The complimentary strain energy, U^*, was obtained by integration of the complimentary strain energy density, u_0^*, in the beam volume:

$$U^* = \int_{-h_2}^{0} u_0^* bad z_1 + \int_{-h_2}^{0} u_0^* b(l-a) dz_1 + \int_{-h_1-h_2}^{-h_2} u_0^* b(l-a) dz_1. \tag{36}$$

The complimentary strain energy density is equal to the area OQR that supplements the area OPQ to a rectangle (Fig. 3). Therefore, the complimentary strain energy density was written as

$$u_0^* = \sigma\varepsilon - u_0. \tag{37}$$

By combining (23), (26) and (37), we obtained

$$u_0^* = Et^2 \left[1 - \frac{1}{\sqrt{1 + \left(\frac{\varepsilon}{t}\right)^2}} \right]. \tag{38}$$

After substitution of (3), (4), (24), (28) and (38) in (36), we derived

$$U^* = abt^2 \left[1 - \frac{1}{\sqrt{1 + \left(\frac{\varepsilon_c}{t}\right)^2}} \right] \frac{h_2}{3} (2E_{c0} + E_{c1}) + \frac{1}{3} b(l-a) t^2 \left[1 - \frac{1}{\sqrt{1 + \left(\frac{\varepsilon_d}{t}\right)^2}} \right] \left[h_2 (2E_{c0} + E_{c1}) + h_1 \left(2E_{f0} + E_{f1}\right) \right] \tag{39}$$

The expression obtained by combining (34), (35) and (39) was doubled, since there are two symmetric cracks (Fig. 1):

$$G = 2t^2 \left[1 - \frac{1}{\sqrt{1 + \left(\frac{\varepsilon_c}{t}\right)^2}} \right] \frac{h_2}{3} \left(2E_{c0} + E_{c1}\right) + \frac{2}{3} t^2 \left[\frac{1}{\sqrt{1 + \left(\frac{\varepsilon_d}{t}\right)^2}} - 1 \right] \left[h_2 \ (2E_{c0} + E_{c1}) + \ h_1 \left(2E_{f0} + E_{f1}\right) \right]. \tag{40}$$

The fact that (40) is exact match of (31) verifies the J-integral non-linear solution (31).

Finally, a non-linear fracture analysis of the three-layered functionally graded beam (Fig. 1) was performed assuming that the modulus of elasticity, $E_c(z_1)$, in the internal layer I varies according to the following exponential law:

$$E_c(z_1) = E_{c0} e^{-\lambda z_1}, \lambda \geq 0 \ \text{ at } \ -h_2 \leq z_1 \leq 0, \tag{41}$$

where E_{c0} is the modulus in the beam cross-sectional centre.

The modulus of elasticity, $E_f(z_1)$, of the external layer II was written as

$$E_f(z_1) = E_{f0} e^{-\lambda(h_2 + z_1)}, \ \ \text{at} -h_1 - h_2 \leq z_1 \leq -h_2, \tag{42}$$

where E_{f0} is the modulus in the lower edge of layer II.

The stress-strain relation (23) was used to describe the non-linear material behaviour in layer I (for this purpose, E was replaced with (41)). Equation (23) was applied also in layer II (the modulus, E, was replaced with (42)).

Equation (5) was applied to obtain the J-integral components in segment A_1 (Fig. 1). For this purpose, σ was found by substitution of (41) in (23).

The longitudinal strain, ε_c, in the internal crack arm behind the crack tip was obtained from Eq. (7). By combining (7), (23) and (41), we derived

$$\varepsilon_c = \frac{t\theta}{\sqrt{t^2 - \theta^2}}, \ \ \theta = \frac{F\lambda}{2bE_{c0}(e^{\lambda h_2} - 1)}. \tag{43}$$

After substitution of (5), (10), (11), (23), (26), (41) and (43) in (1), we obtained

$$J_{A_1} = t^2 \left[1 - \frac{1}{\sqrt{1 + \left(\frac{\varepsilon_c}{t}\right)^2}} \right] \frac{E_{c0}}{\lambda} \left(e^{\lambda h_2} - 1\right). \tag{44}$$

Equation (13) was used to determine the J-integral components in segment B_1 (σ was obtained by substitution of (41) in (23)).

The longitudinal strain, ε_d, in the un-cracked beam portion was found by substitution of (23), (41) and (42) in (15):

$$\varepsilon_d = \frac{t\zeta}{\sqrt{t^2-\zeta^2}}, \zeta = \frac{F\lambda}{2b\left[E_{c0}\left(e^{\lambda h_2}-1\right)+E_{f0}\left(e^{\lambda h_1}-1\right)\right]} \tag{45}$$

By combining (1), (11), (13), (23), (26), (41) and (45), we derived

$$J_{B_1} = t^2\left[\frac{1}{\sqrt{1+\left(\frac{\varepsilon_d}{t}\right)^2}}-1\right]\frac{E_{c0}}{\lambda}\left(e^{\lambda h_2}-1\right). \tag{46}$$

In segment B_2, the J-integral components were found by (13) (the stress, σ, was determined by substitution of (42) in (23)). The strain energy density was calculated by substitution of (42) in (26).

By combining of (1), (11), (23), (26), (42) and (45), we derived

$$J_{B_2} = t^2\left[\frac{1}{\sqrt{1+\left(\frac{\varepsilon_d}{t}\right)^2}}-1\right]\frac{E_{f0}}{\lambda}\left(e^{\lambda h_1}-1\right). \tag{47}$$

Equations (44), (46) and (47) were substituted in (2):

$$J = 2t^2\left[1-\frac{1}{\sqrt{1+\left(\frac{\varepsilon_c}{t}\right)^2}}\right]\frac{E_{c0}}{\lambda}\left(e^{\lambda h_2}-1\right)+ +2t^2\left[\frac{1}{\sqrt{1+\left(\frac{\varepsilon_d}{t}\right)^2}}-1\right]\left[\frac{E_{c0}}{\lambda}\left(e^{\lambda h_2}-1\right)+\frac{E_{f0}}{\lambda}\left(e^{\lambda h_1}-1\right)\right], \tag{48}$$

where ε_c and ε_d were calculated by (43) and (45), respectively.

A non-linear strain energy release rate analysis was conducted in order to verify (48). After substitution of (38), (41), (42), (43) and (45) in (36), the beam complimentary strain energy was written as

$$U^* = abt^2\left[1-\frac{1}{\sqrt{1+\left(\frac{\varepsilon_c}{t}\right)^2}}\right]\frac{E_{c0}}{\lambda}\left(e^{\lambda h_2}-1\right) + b(l-a)t^2\left[1-\frac{1}{\sqrt{1+\left(\frac{\varepsilon_d}{t}\right)^2}}\right]\left[\frac{E_{c0}}{\lambda}\left(e^{\lambda h_2}-1\right)+\frac{E_{f0}}{\lambda}\left(e^{\lambda h_1}-1\right)\right]. \tag{49}$$

After combining (34), (35) and (49), the expression obtained was doubled:

$$G = 2t^2\left[1-\frac{1}{\sqrt{1+\left(\frac{\varepsilon_c}{t}\right)^2}}\right]\frac{E_{c0}}{\lambda}\left(e^{\lambda h_2}-1\right) + 2t^2\left[\frac{1}{\sqrt{1+\left(\frac{\varepsilon_d}{t}\right)^2}}-1\right]\left[\frac{E_{c0}}{\lambda}\left(e^{\lambda h_2}-1\right)+\frac{E_{f0}}{\lambda}\left(e^{\lambda h_1}-1\right)\right], \tag{50}$$

which is exact match of (48). This fact is a verification of non-linear solution (48).

Further, it was assumed that the beam configuration in Fig. 1 is made of an arbitrary number of functionally graded layers composed symmetrically with respect to the centroid. Therefore, only the upper half of beam, $-h/2 \le z_1 \le 0$, was analysed. Perfect adhesion was assumed between layers. Each layer has individual thickness and material properties. The material behaviour in each layer was described by the non-linear stress-strain law (23). In each layer, the material is functionally graded along the layer thickness. It was assumed that the modulus of elasticity, E_i, in each layer varies continuously along the layer thickness according to the following quadratic law:

$$E_i(z_1) = E_{ai} + \frac{E_{bi}-E_{ai}}{\left(z_{1i+1}-z_{1i}\right)^2}(z_1-z_{1i})^2 \text{at } z_{1i} \le z_1 \le z_{1i+1}, \tag{51}$$

where E_{ai} and E_{bi} are, respectively, the moduli of elasticity in the upper and lower edge of the ith layer and z_{1i} and z_{1i+1} are, respectively, the coordinates of the upper and lower edge of the same layer.

The non-linear fracture behaviour was studied in terms of the strain energy release rate by using formula (34). In order to determine the complimentary strain energy, formula (36) was re-written as

$$U^* = \sum_{i=1}^{i=n_c}\int_{z_{1i}}^{z_{1i+1}} u_{0i}^* b a dz_1 + \sum_{i=1}^{n}\int_{z_{1i}}^{z_{1i+1}} u_{0i}^* b(l-a)dz_1, \tag{52}$$

where n_c and n are the layer number in the internal crack arm and in the un-cracked beam portion, respectively. The strain energy density in the ith layer, u_{0i}^*, was written as

$$u_{0i}^* = \sigma_i\varepsilon - u_{0i}, \tag{53}$$

where σ_i and u_{0i} are the stress and the strain energy density, respectively. The stress in each layer was calculated by applying the non-linear stress-strain relation (23). In order to determine the strain, ε_c, in the internal crack arm in the equilibrium, Eq. (7) was re-written as

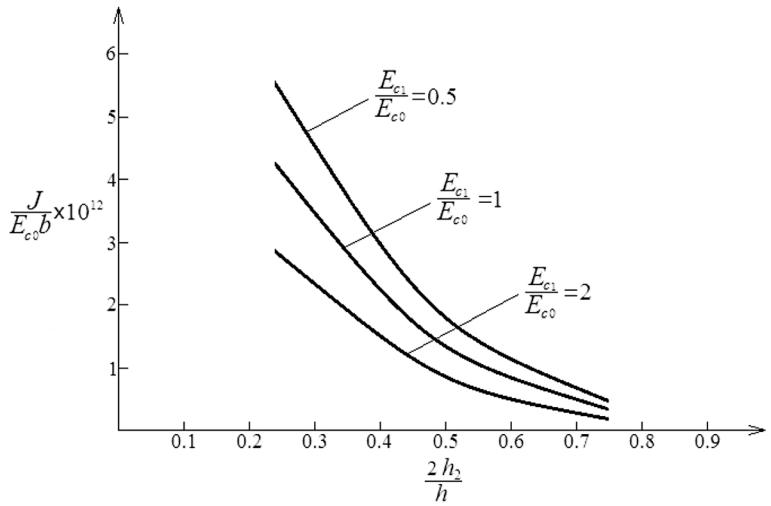

Fig. 4 The *J*-integral value in non-dimensional form plotted against $2h_2/h$ ratio at different E_{c1}/E_{c0} ratio. The modulus of elasticity varies along the beam height according to quadratic laws (3) and (4)

$$\frac{F}{2}=\sum_{i=1}^{i=n_c}\int_{z_{1i}}^{z_{1i+1}}\sigma_i b dz_1. \tag{54}$$

By combining (23), (51) and (54), we derived

$$\varepsilon_c=\frac{t\psi}{\sqrt{t^2-\psi^2}}, \tag{55}$$

where

$$\psi=\frac{3F}{2b\sum_{i=1}^{i=n_c}(z_{1i+1}-z_{1i})(2E_{ai}+E_{bi})}. \tag{56}$$

The strain, ε_d, in the un-cracked beam portion, $x \geq 0$, was found from the following equilibrium equation:

$$\frac{F}{2}=\sum_{i=1}^{n}\int_{z_{1i}}^{z_{1i+1}}\sigma_i b dz_1. \tag{57}$$

After substituting (23) and (51) in (56), we obtained

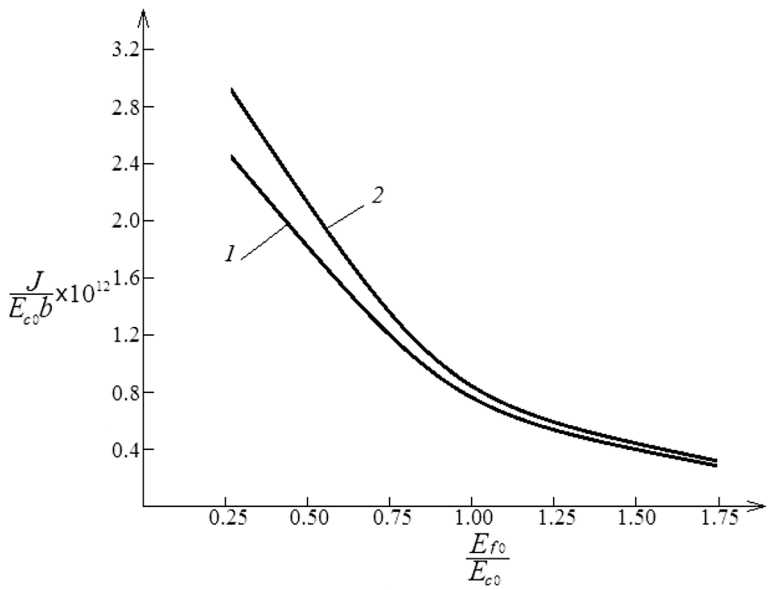

Fig. 5 The *J*-integral value in non-dimensional form plotted against E_{f0}/E_{c0} ratio (*curve 1* linear-elastic material behaviour, *curve 2* elastic-plastic material behaviour). The modulus of elasticity varies along the beam height according to quadratic laws (3) and (4)

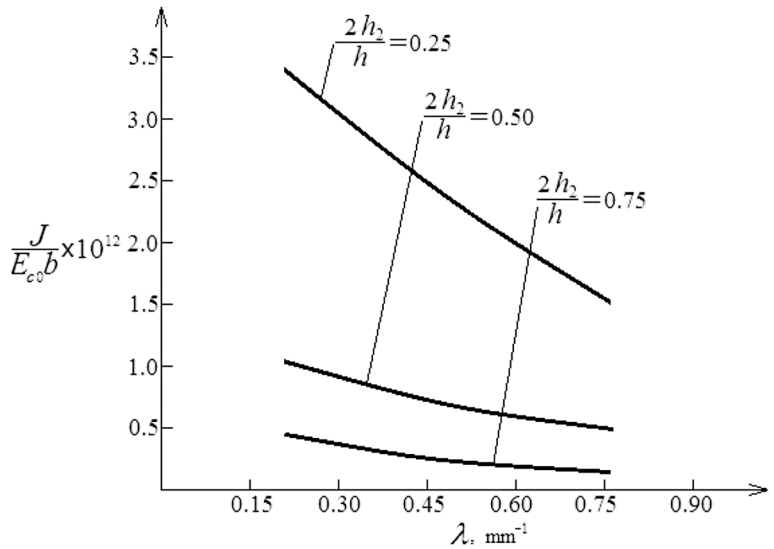

Fig. 6 The *J*-integral value in non-dimensional form plotted against the power law exponent, λ, at different $2h_2/h$ ratios. The modulus of elasticity varies along the beam height according to exponential laws (41) and (42)

$$\varepsilon_d = \frac{t\eta}{\sqrt{t^2-\eta^2}}, \tag{58}$$

where

$$\eta = \frac{3F}{2b\sum_{i=1}^{i=n}(z_{1i+1}-z_{1i})(2E_{ai}+E_{bi})}. \tag{59}$$

Finally, by doubling the result derived by substituting (23), (35), (51), (52), (53), (55) and (58) in (34), we found the following formula for the strain energy release rate:

$$G = \frac{2}{3}t^2\left[1-\frac{1}{\sqrt{1+\left(\frac{\varepsilon_c}{t}\right)^2}}\right]\sum_{i=1}^{i=n_c}(z_{1i+1}-z_{1i})(2E_{ai}+E_{bi}) + \frac{2}{3}t^2\left[\frac{1}{\sqrt{1+\left(\frac{\varepsilon_d}{t}\right)^2}}-1\right]\sum_{i=1}^{i=n}(z_{1i+1}-z_{1i})(2E_{ai}+E_{bi}), \tag{60}$$

where ε_c and ε_d are determined by (55) and (58), respectively.

Results

The effects were evaluated of crack location along the beam height and material properties on the non-linear mode II delamination fracture behaviour of the functionally graded three-layered beam configuration considered. The crack location along the beam height was characterized by $2h_2/h$ ratio (Fig. 1). First, the *J*-integral non-linear solution (31) derived for quadratic law of variation of modulus of elasticity along the beam height was analysed. For this purpose, the *J*-integral value was calculated at various $2h_2/h$ ratios for $E_{c1}/E_{c0} = 0.5$, 1 and 2. In these calculations, it was assumed that $h = 0.004$ m, $b = 0.02$ m, $F = 30$ N, $t = 1$, $E_{f0}/E_{c0} = 1.2$ and $E_{f1}/E_{f0} = 0.8$. The *J*-integral values generated were presented in non-dimensional form by using the formula $J_N = J/(E_{c0}b)$ and plotted against $2h_2/h$ ratio as shown in Fig. 4. The diagrams in Fig. 4 indicate that the *J*-integral value decreases with increasing $2h_2/h$ ratio. This finding was attributed to increase the

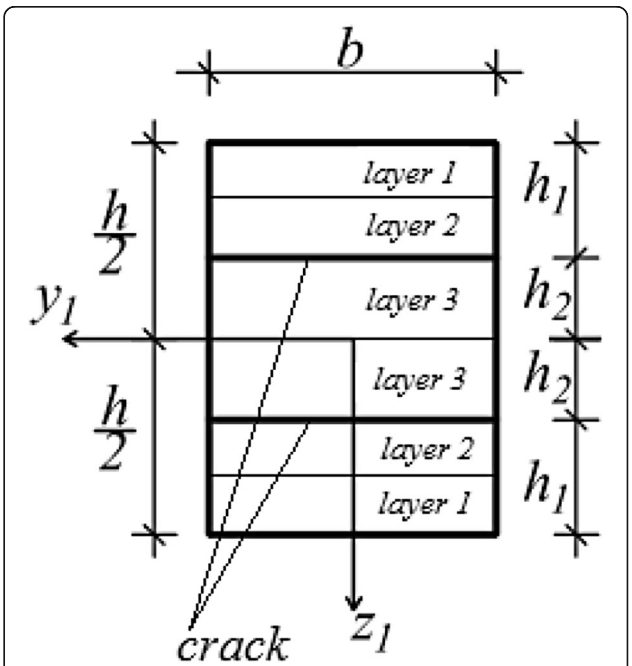

Fig. 7 The cross section of a six-layer beam configuration

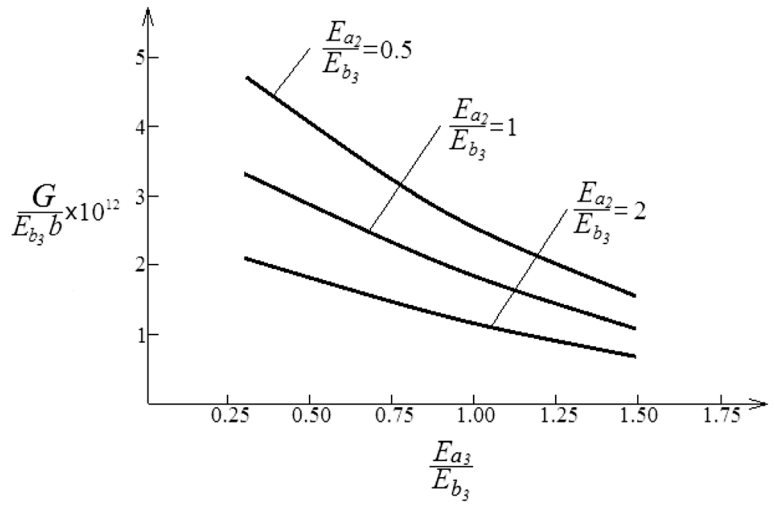

Fig. 8 The strain energy release rate in non-dimensional form plotted against E_{a3}/E_{b3} ratio for three values of E_{a2}/E_{b3} ratio for the six-layer beam configuration

internal crack arm stiffness. One can observe also (Fig. 4) that the increase of E_{c1}/E_{c0} ratio leads to decrease of the *J*-integral value (this is due to increase of the beam stiffness).

The influence of E_{f0}/E_{c0} ratio on the fracture behaviour was analysed too. For this purpose, the *J*-integral value was plotted in non-dimensional form against E_{f0}/E_{c0} ratio for $E_{c1}/E_{c0} = 2$, $E_{f1}/E_{f0} = 0.8$ and $2h_2/h = 3/4$ as illustrated in Fig. 5. It can be observed that the *J*-integral value decreases with increasing E_{f0}/E_{c0} ratio, which can be explained with increase of the beam stiffness. The *J*-integral values obtained by the linear-elastic solution (22) at various E_{f0}/E_{c0} ratios for $E_{c1}/E_{c0} = 2$, $E_{f1}/E_{f0} = 0.8$ and $2h_2/h = 3/4$ were presented also in Fig. 5 in non-dimensional form in order to evaluate the influence of material non-linearity on the mode II fracture behaviour. One can observe in Fig. 5 that the material non-linearity leads to increase of the *J*-integral value. Therefore, the non-linear behaviour of material has to be taken into account in fracture mechanics-based safety design of structural members composed by functionally graded materials.

The effects of crack location and material properties on the non-linear mode II fracture behaviour were investigated also when the modulus of elasticity varies along the beam height according to the exponential laws (41) and (42). The *J*-integral value was calculated by non-linear solution (48) at various λ for $2h_2/h = 0.25$, 0.50 and 0.75, and $E_{f0}/E_{c0} = 1.1$. The results are

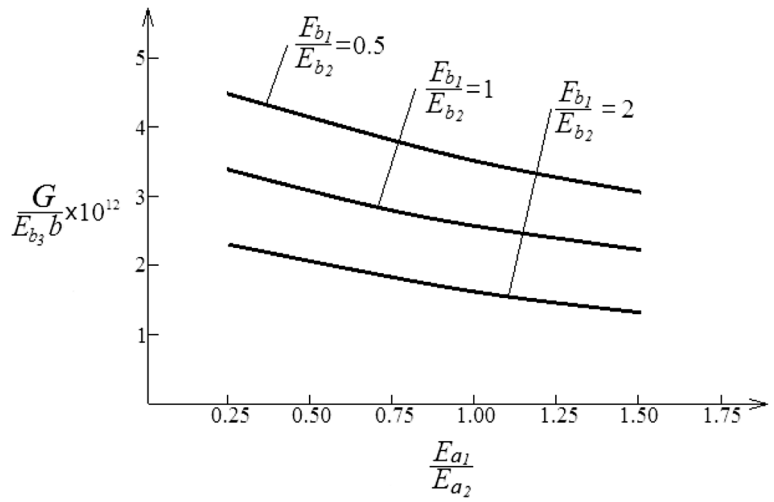

Fig. 9 The strain energy release rate in non-dimensional form presented as a function of E_{a1}/E_{a2} ratio for three values of E_{b1}/E_{b2} ratio for the six-layer beam configuration

presented in non-dimensional form in Fig. 6. The data in Fig. 6 indicate that the *J*-integral value decreases with increasing λ. This fact is explained with increase of the exponent in (41) and (42), since $z_1 < 0$. It can be observed also that increase of $2h_2/h$ ratio leads to decrease of the *J*-integral value (Fig. 6).

The effects of material gradient on the mode II non-linear delamination fracture behaviour of multilayered beam were also analysed. A beam configuration made of six layers composed symmetrically with respect to the centroid was considered (the beam cross section is shown schematically in Fig. 7). The thickness of layers 1 and 2 is equal to $h_1/2$. The thickness of layer 3 is h_2. The influence of material gradient along the thickness of layer 3 was investigated. For this purpose, the strain energy release rate was calculated by applying formula (60). The material gradient was characterized by E_{a3}/E_{b3} ratio. The results obtained were presented in non-dimensional form by using formula, $G_N = G/(E_{b3}b)$. The strain energy release rate in non-dimensional form was plotted against E_{a3}/E_{b3} ratio for three values of E_{a2}/E_{b3} ratio in Fig. 8. One can observe in Fig. 8 that the strain energy release rate decreases with increasing of E_{a3}/E_{b3} and E_{a2}/E_{b3} ratios. This was explained with the increase of beam stiffness. Further, the influence of E_{a1}/E_{a2} and E_{b1}/E_{b2} ratios on the delamination fracture was also evaluated. For this purpose, the strain energy release rate in non-dimensional form was presented as a function of E_{a1}/E_{a2} ratio for three values of E_{b1}/E_{b2} ratio in Fig. 9. The curves in Fig. 9 indicate that the increase of E_{a1}/E_{a2} and E_{b1}/E_{b2} ratios leads to decrease of the strain energy release rate.

Conclusions

First, the mode II delamination fracture behaviour of a functionally graded three-layered beam exhibiting material non-linearity was studied theoretically. There were two delamination cracks located symmetrically with respect to the beam centroid. The internal crack arm was loaded centrically by one tensile force. The material was functionally graded along the beam height. Two laws (quadratic and exponential) for variation of the modulus of elasticity were considered in the fracture analysis. The beam mechanical behaviour was described by using a non-linear stress-strain relation. The fracture was analysed by applying the *J*-integral approach. Closed form analytical solutions of the *J*-integral were derived for the two laws of variation of modulus of elasticity. Analyses of the strain energy release rate were developed with taking into account the material non-linearity in order to verify the *J*-integral non-linear solutions derived. The non-linear mode II delamination fracture was also analysed assuming that the beam under consideration is multilayered (in each layer, the material is functionally graded in the thickness direction). The effects of material gradient, crack location along the beam height and material non-linearity on the mode II delamination fracture behaviour of functionally graded three-layered beam configuration were evaluated. The results obtained can be applied for optimization of the beam structure in its design with respect to the non-linear fracture performance. Comparisons were carried out between linear-elastic and elastic-plastic fracture behaviour. It was found that the material non-linearity leads to increase of the *J*-integral value. Therefore, the material non-linearity has to be considered in fracture mechanics-based safety design of structural members composed by functionally graded materials. The present study indicates that the analytical approach can be applied to obtain very useful information for mode II non-linear fracture behaviour, since the simple formulae derived capture the essential of material non-linearity.

Acknowledgements
The present study was supported financially by the Research and Design Centre (CNIP) of the UACEG, Sofia (Contract BN – 189/2016).

Author's information
Victor Iliev Rizov
Office Address: Department of Technical Mechanics, University of Architecture, Civil Engineering and Geodesy, 1 Chr. Smirnensky Blvd., Sofia - 1046 Bulgaria
fax: +(359-2) 86 56 863
e-mail: v_rizov_fhe@uacg.bg
1. Education
   1983–1988: Higher Institute of Civil Engineering and Architecture - Sofia
   1995: Doctor of Philosophy in Mechanics of Materials; University of Architecture, Civil Engineering and Geodesy, Sofia
2. Personal career
   1989–1996: Assistant Professor
   1996–2004: Senior Assistant Professor
   2004–2013: Associate Professor
   2013–present: Professor
3. Major subjects of research
   Non-linear fracture mechanics
   Non-linear behaviour of sandwich structures
   Mechanics of fibre reinforced composites
   Elastic-plastic behaviour of structures
4. Publications
   More than 120 publications

Competing interests
The author declares that he has no competing interests.

Received: 28 October 2016 Accepted: 23 January 2017
Published online: 01 February 2017

References

Anlas, G., Santare, M. H., & Lambros, J. (2000). Numerical calculation of stress intensity factors in functionally graded materials. *International Journal of Fracture, 104*(2), 131–143.

Ashrafi, H., & Shariyat, M. (2014). A numerical boundary integral equation analysis for standard linear viscoelastic media made of functionally graded materials. *International Journal of Mechanical and Materials Engineering, 9*(9). doi:10.1186/s40712-014-0009-4.

Bohidar, S. K., Sharma, R., & Mishra, P. R. (2014). Functionally graded materials: a critical review. *International Journal of Research, 1*(7), 289–301.

Butcher, R. J., Rousseau, C. E., & Tippur, H. V. (1999). A functionally graded particulate composite: measurements and failure analysis. *Acta Materialia, 47*(2), 259–268.

Carpinteri, A., & Pugno, N. (2006). Cracks in re-entrant corners in functionally graded materials. *Engineering Fracture Mechanics, 73*(2), 1279–1291.
Chakrabarty, J. (2006). *Theory of plasticity*. Oxford: Elsevier Butterworth-Heinemann.
Erdogan, F. (1995). Fracture mechanics of functionally graded materials. *Comp. Eng, 5*(7), 753–770.
Gasik, M. M. (2010). Functionally graded materials: bulk processing techniques. *International Journal of Materials and Product Technology, 2010*(1-2), 20–29. No 39.
Hirai, T., & Chen, L. (1999). Recent and prospective development of functionally graded materials in Japan. *Materials Science Forum, 308–311*, 509–514.
Ivanov, Y., & Stoyanov, V. (2011). High technologies and new construction materials in civil engineering. In *Education, Science, Innovations* (pp. 161–169). Pernik: Proc. Ist Int. Conf. of the European Polytechnical University.
Lu, C. F., Lim, C. W., & Chen, W. Q. (2009). Semi-analytical analysis for multi-dimensional functionally graded plates: 3-D elasticity solutions. *Int. J. Num. Meth. Engng, 79*(3), 25–44.
Maganti, N. V. R., & Nalluri, M. R. (2015). Flapwise bending vibration analysis of functionally graded rotating double-tapered beams. *International Journal of Mechanical and Materials Engineering, 10*(21). doi:10.1186/s40712-015-0040-0.
Mladensky, A., & Rizov, V. (2013). Analytical investigation of nonlinear interlaminar fracture in trilayered polymer composite beam under mode II crack loading conditions using the *J*-integral. *Archive of Applied Mechanics, 83*, 1637–1658.
Mohammadiha, O., & Ghariblu, H. (2016). Multi-objective optimization of functionally graded thickness tubes under external inversion over circular dies. *International Journal of Mechanical and Materials Engineering, 11*(8). doi:10.1186/s40712-016-0061-3.
Mortensen, A., & Suresh, S. (1995). Functionally graded metals and metal-ceramic composites: part 1 processing. *Int. Mater. Rev, 40*(6), 239–265.
Nemat-Allal, M. M., Ata, M. H., Bayoumi, M. R., & Khair-Eldeen, W. (2011). Powder metallurgical fabrication and microstructural investigations of aluminum/steel functionally graded material. *Materials Sciences and Applications, 2*(1), 1708–1718.
Neubrand, A., & Rödel, J. (1997). Gradient materials: an overview of a novel concept. *Zeit f Met, 88*(2), 358–371.
Paulino, G. C. (2002). Fracture in functionally graded materials. *Engng Fract Mech, 69*(2), 1519–1530.
Pei, G., & Asaro, R. J. (1997). Cracks in functionally graded materials. *Int. J. Solids and Structures, 34*(1), 1–17.
Petrov, V. V. (2014). Non-linear incremental structural mechanics. *M.: Infra-Injeneria.*
Pan, S.-D., Feng, J.-C., Zhou, Z.-G., & Wu-Lin-Zhi. (2009). Four parallel non-symetric Mode-III cracks with different lengths in a functionally graded material plane. *Strength, Fracture and Complexity: an International Journal, 5*, 143–166.
Suresh, S., & Mortensen, A. (1998). *Fundamentals of functionally graded materials*. London: IOM Communications Ltd.
Szekrenyes, A. (2010). Fracture analysis in the modified split-cantilever beam using the classical theories of strength of materials. *Journal of Physics: Conference Series, 240*(1), 012030.
Szekrenyes, A., & Vicente, W. M. (2012). Interlaminar fracture analysis in the GII-GIII plane using prestressed transparent composite beams. *Composites Part A Applied Science and Manufacturing, 43*(1), 95–103.
Tilbrook, M. T., Moon, R. J., & Hoffman, M. (2005). Crack propagation in graded composites. *Composite Science and Technology, 65*(2), 201–220.
Tsukamoto, H. (2014). Mechanical properties of zirconia–titanium composites. *International Journal of Materials Science and Applications, 3*(5), 260–267.
Upadhyay, A. K., & Simha, K. R. Y. (2007). Equivalent homogeneous variable depth beams for cracked FGM beams; compliance approach. *International Journal of Fracture, 144*(3), 209–213.